Development and Evaluation of Refreshable Braille Display and Active Touch-Reading System for Digital Reading of the Visually Impaired

Dapeng Chen, *Member, IEEE*, Yunjie Zhang, Xuhui Hu, *Member, IEEE*, Geng Chen, Yingping Fang, Xu Chen, Jia Liu, *Member, IEEE*, and Aiguo Song, *Senior Member, IEEE*

***Abstract*— The traditional way of reading through Braille books is constraining the reading experience of blind or visually impaired (BVI) in the digital age. In order to improve the reading convenience of BVI, this paper proposes a low-cost and refreshable Braille display device, and solves the problems of high energy consumption and low latching force existing in existing devices. Further, the Braille display device was combined with the 3D Systems Touch device to develop an active Braille touch-reading system for digital reading of BVI with the help of the CHAI3D virtual environment. Firstly, according to the actual needs of BVI to touch and read the Braille dots, this paper utilizes the beam structure to provide a full latching function for the raised Braille dot without energy consumption. Through theoretical derivation and finite element analysis, the performance of the Braille dot actuator is optimized to provide sufficient feedback force and latching force for finger's touch-reading. Then, this paper designs a virtual Braille interactive environment based on the CHAI3D, and combines the sense of touch with audio to effectively improve the recognition accuracy and reading efficiency of BVI for Braille through the multi-modal presentation of Braille information. The performance test results of the device show that the average lifting force of the Braille dot actuator is 101.67 mN, the latching force is over 5 N, and the average refresh frequency is 17.1 Hz, which meets the touch-reading needs of BVI. User experiments show that the average accuracy rate of BVI subjects in identifying digitized Braille is 95.5%, and subjects have a high subjective evaluation of the system.**

***Index Terms*— Braille display device, digital reading for the BVI, electromagnetic drive, full latching function, active Braille touch-reading.**

Manuscript received 12 September 2023; revised 11 January 2024; accepted 4 February 2024. Date of publication 7 February 2024; date of current version 28 February 2024. This work was supported in part by the National Natural Science Foundation of China under Grant 62003169 and Grant 62303453; in part by the Natural Science Foundation of Jiangsu Province under Grant BK20200823; in part by the Key Research and Development Program of Jiangsu Province (Industry Prospects and Key Core Technologies) under Grant BE2020006-2; and in part by the Postgraduate Research & Practice Innovation Program of Jiangsu Province under Grant SJCX22_0351, Grant SJCX22_0348, and Grant KYCX22_1202. *(Corresponding authors: Jia Liu; Aiguo Song.)*

This work involved human subjects or animals in its research. Approval of all ethical and experimental procedures and protocols was granted by the Science and Technology Department, Nanjing University of Information Science & Technology.

Dapeng Chen, Yunjie Zhang, Geng Chen, Yingping Fang, Xu Chen, and Jia Liu are with the School of Automation, C-IMER, CICAEET, B-DAT, Nanjing University of Information Science & Technology, Nanjing 210044, China (e-mail: dpchen@nuist.edu.cn; liujia@nuist.edu.cn).

Xuhui Hu is with the Suzhou Institute of Biomedical Engineering and Technology (SIBET), Chinese Academy of Sciences (CAS), Suzhou 215163, China.

Aiguo Song is with the School of Instrument Science and Engineering, Southeast University, Nanjing 210096, China (e-mail: a.g.song@seu.edu.cn).

Digital Object Identifier 10.1109/TNSRE.2024.3363495

I. Introduction

BLIND or visually impaired (BVI) are persons with complete loss or severe impairment of vision. According to a report by the Global Health Committee of The Lancet on global eye health, there were approximately 43 million blind people worldwide in 2020, and it will increase to 61 million in 2050 [1]. Due to severe vision impairment, BVI mainly rely on touch [2], [3], [4] and hearing [5] to gather information from their surroundings. In terms of reading, BVI can not only listen to books by voice, but also read Braille with fingers. Compared with reading Braille by touch, obtaining information through voice is easily restricted by the environment [6], and long-term dependence on voice will also cause certain damage to hearing. Therefore, BVI mainly relies on fingers to touch Braille for reading [7]. Currently, the predominant tools for Braille reading in BVI is still paper-based Braille books. However, these paper-based tools suffer from drawbacks such as bulkiness, high cost, limited availability, and susceptibility to damage, which have gradually made them inadequate for meeting the reading needs of BVI [8].

With the advancement of technology, numerous studies have attempted to design Braille display devices with adjustable Braille dot states according to the technical specifications of Braille characters, replacing Braille books as digital reading tools for BVI. The stimulation forms of Braille dots to finger skin mainly include electrotactile and pressure. Among them, the electrotactile Braille display device has the advantages of

simple structure, small size, and low power consumption [9]. However, the tingling sensation caused by electrical stimulation and the unstable Braille display effect caused by finger sweating are issues that need to be further addressed by such devices [10], [11].

Currently, pressure-stimulated Braille display devices are more commonly used, which mainly employed air pressure [12], [13], deformable materials, and electromagnetic forces to drive Braille dot actuators. For example, pneumatic actuators are usually driven by a high-pressure air pump through pressure control valves and intricate air ducts to drive and maintain the protrusion of Braille dots [14], [15], resulting in larger device sizes, limited portability, and higher energy consumption.

Braille display devices driven by deformable materials mainly utilize thermosensitive shape memory alloys (SMAs) [16], as well as electroactive polymers [17], [18] and piezoelectric materials that are sensitive to electricity. Among them, SMAs have slow deformation speed and low fatigue resistance [8], making it difficult to meet the long-term use needs of Braille dots. Chakraborti et al. [19] tried to use electroactive polymers to develop Braille dot actuators, but it can only provide a maximum feedback force of 50 mN after raise, which is difficult to meet the requirements of practical use. In addition, the device needs to be activated under a high-voltage electric field of 100 kV/mm, posing a potential safety risk to BVI. In contrast, piezoelectric actuators have more advantages in making Braille display devices. For example, Metec Ingenieur AG in Germany has launched the Braille-line-Flat 20 [20] model of the Braille display device. The device is driven by the piezoelectric actuator, with a feedback force of over 170 mN and a Braille dot rise time of only 50 ms. However, the price of these commercial Braille display devices is generally high [7], [8]. In addition, there are some special ways to drive Braille dots. For instance, Paneva et al. [21] developed a Braille display device that can emit point-shaped ultrasonic radiation pressure to the palm of the BVI.

In order to make Braille display devices reliable in performance, fast in response, low in cost, and high in feedback force, a great deal of research has developed Braille dot actuators driven by electromagnetic force. For example, Chen et al. [22] implemented a layered electromagnetic driving mechanism to achieve dense arrangement of Braille dots, and provided a latching force greater than 150 mN for raised Braille dots through continuous energy supply. Bettelani et al. [23] developed a semi-latching single-cell Braille display device based on the principle of electromagnetic drive for displaying letters and numbers. To accommodate the tactile sensitivity of diverse learners, Saikot and Sanim [24] designed a Braille display device with adjustable Braille cell size using electromechanical baffle actuator. They also introduced voice functionality, allowing BVI to independently operate the Braille display device. The aforementioned electromagnetic Braille dot actuators all employ a semi-latching structure. However, due to the poor self-locking ability, devices with a semi-latching structure often require continuous power supply to the raised Braille dots to maintain their state, resulting in high energy consumption and high heat generation. Additionally, when the fingertip's pressing force exceeds the latching force provided by the Braille dots, the information displayed on these devices will be altered and convey incorrect Braille information to the BVI. Therefore, ensuring sufficient latching force for raised Braille dots is crucial for the reliability of Braille display devices.

To maintain the state of raised Braille dots, some studies have designed fully latched Braille dot structures. This structure adopts a mechanical locking method, which effectively reduces the energy consumption of the device by avoiding continuous energy supply when the Braille dots raised. For example, Loconsole et al. [25] designed a fully latched Braille display device with 40 Braille cells using magnetically conductive metal pins, and sequentially changed the raised state of Braille dots arranged in row by moving a single electromagnetic driven cursor. Although this device avoids designing a drive unit for each Braille dot actuator separately, the movement speed of the cursor cannot be too fast, resulting in a refresh rate of only 0.07 Hz. Kim et al. [26] developed a fully latched Braille display device using a flip-latch structure, which not only meets the latching force requirements for Braille reproduction, but also does not consume additional energy during latching. However, the lifting force of the Braille dot in the device is less than 10 mN, which may cause the Braille dots to fail to bounce when the fingers are in contact with them.

Referring to the Braille standard and existing research, it can be seen that Braille dots not only have small diameters and dense arrangements, but also meet certain technical requirements in terms of protrusion height, refresh frequency, lifting force, and latching force. Therefore, this paper aims to design a low-cost full latching Braille dot actuator using electromagnetic driving principles to accurately convey Braille information to BVI and reduce energy consumption. This paper adopts a beam structure to achieve the full latching function of the Braille dot actuator and utilizes finite element analysis to simulate and optimize its structure. The goal is to equip the actuator with advantages such as high latching force, compact size, low energy consumption, and cost-effectiveness.

Furthermore, to enhance digital reading for BVI, this paper integrates the proposed Braille display device with the 3D Systems Touch device [27], and develops a Braille touch-reading system for BVI digital reading in conjunction with the CHAI3D virtual environment. The CHAI3D-based virtual Braille interactive environment displays Braille cells according to the layout and structure of Braille book page, and utilizes attraction constraint method [28] to maintain continuous contact between virtual proxy point and the Braille line. Simultaneously, a force-guidance mechanism [29] is introduced into the haptic rendering of Braille interaction to guide the line-breaking or page-changing operations of BVI in the virtual environment, thereby ensuring that the proposed Braille touch-reading system has high accessibility and convenience for BVI [30]. In addition, by combining haptic feedback with auditory cues [31], multi-modal presentation of Braille information enhanced BVI's understanding of the read content and improved the Braille reading efficiency. The results of performance tests and user experiments show that the Braille

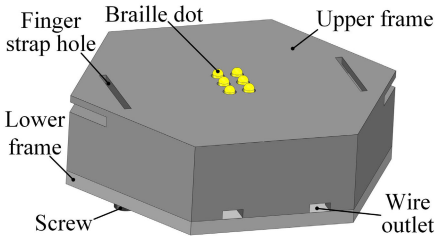

(a) Appearance structure

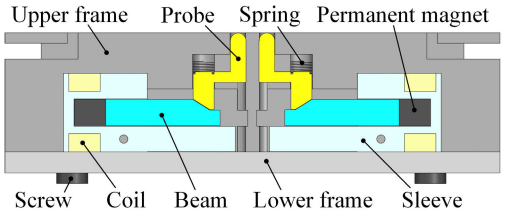

(b) Cross-sectional view

Fig. 1. Schematic diagram of the proposed Braille module.

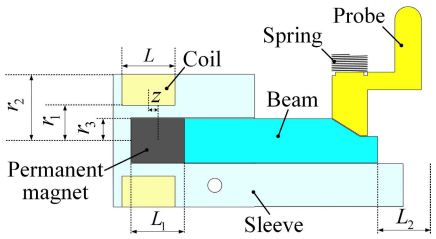

Fig. 2. Simplified geometric structure of Braille dot actuator.

TABLE I
DESIGN PARAMETERS OF BRAILLE DISPLAY DEVICE

Design parameters	Reference value
Dot diameter	1.0-1.6 mm
Dot displacement	0.2-0.5 mm
Dot pitch	2.2-2.8 mm
Latching force	>100 mN
Refresh frequency	>10 Hz for single-line, >1 Hz for multiline

touch-reading system developed in this paper significantly improves the digital reading capabilities of BVI, and provides an effective way for BVI to read digital texts conveniently.

II. Design of Refreshable Braille Display Device

A. Overall Structural Design

The "cell" of standard Braille is an array of dots in 3 rows and 2 columns. BVI reads the information by touching the combined state of 6 Braille dots in one cell. To facilitate BVI's digital reading through a refreshable Braille cell, this paper develops a small refreshable Braille display device. The device is mainly composed of a Braille module and a control unit. Fig. 1(a) shows the appearance structure of the Braille module, which includes the upper frame, Braille dot, finger strap hole, lower frame, screw, and wire outlet. There are 6 Braille dot actuators installed inside the upper frame. The upper and lower frames are fixed with screws. Fig. 1(b) is a cross-sectional view of the Braille module. It can be seen that the Braille dot actuator consists of a probe, spring, permanent magnet, coil, beam, and sleeve. The bottom slope of the probe matches the slope at one end of the beam. The other end of the beam is fixed together with the permanent magnet. The frame, probe, beam and sleeve are all made of resin by 3D printing. The permanent magnet is a cylinder made of neodymium iron boron N38 material. The coil is made of enameled copper wire wound on the sleeve.

B. Design and Working Principle of Braille Dot Actuator

The Braille dot actuator is designed according to the Chinese Braille standard (GB/T 15720-2008) and the parameter standard given in literature [8] (Table I). The shape of Braille dots is hemispherical, with a dot diameter of 1.5 mm, dot displacement of 0.5 mm, and dot pitch of 2.5 mm. Fig. 2 shows a simplified geometric structure diagram of the Braille dot actuator, where the inner radius of the coil is r_1, the outer radius is r_2, and the length is L; the radius of the permanent magnet is r_3, the length is L_1, and the maximum stroke is L_2; z is the distance from the center of the coil to the center of the permanent magnet.

The Braille module achieves latching of raised Braille dots through the beam structure. Fig. 3 illustrates the working principle of this actuator. When not in operation (Fig. 3(a)), the permanent magnet is located on the outside of the sleeve, and the Braille dot is below the contact surface. When the Braille dot needs to rise (Fig. 3(b)), forward current is fed into the coil. At this time, the magnetic field distribution of the coil is N-pole on the outside and S-pole on the inside. Since the outer side of the permanent magnet is the N-pole and the inner side is the S-pole, a repulsive force is generated between the coil and the permanent magnet. The permanent magnet drives the beam to move horizontally inward under the action of repulsive force.

Using the inclined plane of the beam and the probe, the horizontal displacement of the beam is converted into the vertical displacement of the probe, causing the probe to overcome gravity and bounce up. At the same time, the spring is compressed with the vertical movement of the probe. After the stroke of the beam is completed, the probe reaches the highest position (Fig. 3(c)). Meanwhile, the inner end of the beam is inserted into the groove of the upper frame, form a beam structure. At this time, there is no need to inject current into the coil. This is due to the fact that when the finger presses the raised probe downwards, the beam structure provides sufficient latching force to prevent the probe from being pressed down.

When the Braille dot is reset (Fig. 3(d)), reverse current is applied to the coil. At this point, the coil and permanent magnet attract each other due to the opposite direction of the magnetic field, and the permanent magnet drives the beam to move horizontally in reverse. When the beam moves outward, the probe releases the latching state under its own gravity and spring thrust, and moves downward. Finally, the

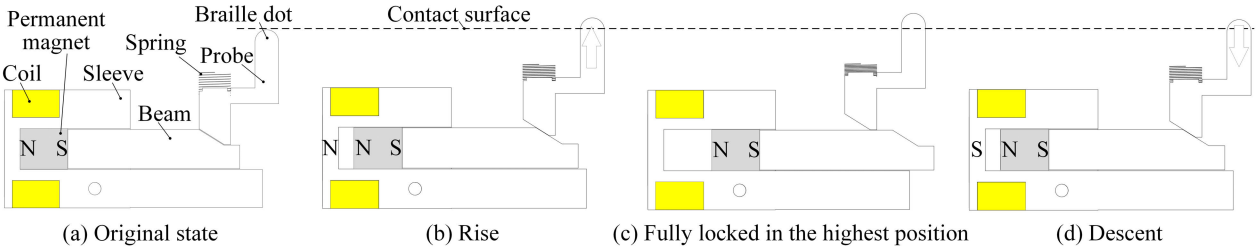

Fig. 3. Working principle of the Braille dot actuator.

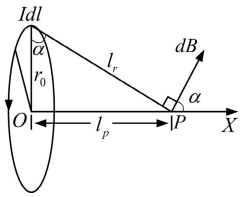

Fig. 4. The axial magnetic field of a circular loop.

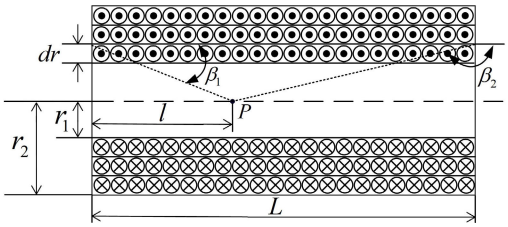

Fig. 5. Electromagnetic coil model.

probe descends to its lowest position and completes the reset.

C. Electromagnetic Design and Finite Element Simulation

The motion performance of the Braille dot actuator is mainly affected by the electromagnetic characteristics between the hollow solenoid (the combination of the coil and the sleeve) and the magnet. After determining the structure, we carried out electromagnetic design and finite element simulation of the Braille dot actuator to obtain the actuator parameters that meet the design requirements. We first carried out a detailed theoretical derivation of the magnetic field of the coil and the permanent magnet, including the force of the probe at different positions. Then, by setting the target lifting force, we derived the electromagnetic force acting on the permanent magnet, and determined the minimum magnetomotive force applied to the coil through simulation analysis. Subsequently, we input the obtained magnetomotive force and related parameter values into the electromagnetic force calculation formula to further calculate the thickness of the coil. Finally, according to the specific geometric parameters, we made prototypes of Braille dot actuators and Braille module, and tested their performance.

1) Magnetic Field Analysis of Coil: The circular loop is a single turn circular circuit distributed by line current, as shown in Fig. 4. Assuming the center of the circular loop is point O, with a radius of r_0, the magnetic flux density generated by an infinitesimal current element at any point on the loop is dB at a point P on the symmetry axis. Due to the axial symmetry of the circular loop, components in the non-axial direction at point P cancel each other out. Therefore, it is only necessary to calculate the magnetic field component along the axis. The total magnetic flux density B of point P is the algebraic sum of the magnetic field components along the axis.

According to Biot-Savart Law, for point P on the axis, let l_p be the distance from point P to the center O. Thus $l_p = l_r \sin\alpha$, B can be calculated as follows:

$$B = \frac{\mu_0 {r_0}^2 I}{2\sqrt{({r_0}^2 + {l_p}^2)^3}}, \tag{1}$$

where $\mu_0 = 4\pi \times 10^{-7}$ H/m is the vacuum permeability.

The essence of the coil is a finite length energized solenoid, which can be analyzed for magnetic field using Biot Savart's law and superposition principle. The finite-length energized solenoid is treated as a circular loop with a steady current. In the case where non-axis magnetic fields cancel each other and only the magnetic field on the axis of the solenoid is considered, a model of the coil composed of multiple layers of windings is established as shown in Fig. 5. The current passing through the coil is I, and the number of turns is N. Point P on the central axis is at a distance l from the left-center point, and dr is the thin layer thickness of the enameled copper wire in the coil, r is the radius of thin layer. The angles formed by point P and dr on the left and right sides of the coil are β_1 and β_2, respectively.

According to equation (1), the magnetic flux density dB generated by the thin layer dr at point P is given by:

$$dB = \frac{\mu_0}{2} j(\cos\beta_1 - \cos\beta_2)dr, \tag{2}$$

where $j = \frac{NI}{L(r_2 - r_1)}$, its physical significance is equivalent to considering the current as a continuous distribution of current density.

Due to $\cos\beta_1 = \frac{l}{\sqrt{l^2+r^2}}$, and $\cos\beta_2 = \frac{l-L}{\sqrt{(L-l)^2+r^2}}$, dB can be obtained as:

$$dB = \frac{\mu_0 NI}{2L(r_2 - r_1)}\left(\frac{l}{\sqrt{l^2+r^2}} - \frac{l-L}{\sqrt{(L-l)^2+r^2}}\right)dr. \tag{3}$$

Integrating over the thin layer with radius r yields the magnetic field at point P as follows [32]:

$$B = \frac{\mu_0 NI}{2L(r_2 - r_1)}\int_{r_1}^{r_2}\left(\frac{l}{\sqrt{l^2+r^2}} - \frac{l-L}{\sqrt{(L-l)^2+r^2}}\right)dr$$

$$= \frac{\mu_0 N I}{2L(r_2 - r_1)} \left[l \ln \frac{r_2 + \sqrt{r_2^2 + l^2}}{r_1 + \sqrt{r_1^2 + l^2}} + (L - l) \ln \frac{r_2 + \sqrt{r_2^2 + (L-l)^2}}{r_1 + \sqrt{r_1^2 + (L-l)^2}} \right]. \tag{4}$$

2) Magnetic Field Analysis of Permanent Magnet: When only considering the magnetic field distribution on the coil axis, the analytical formula for the magnetic field on the permanent magnet axis is [33]:

$$B_1 = \frac{B_r}{2} \left(\frac{z_1}{\sqrt{{z_1}^2 + {r_3}^2}} - \frac{z_1 - L_1}{\sqrt{(z_1 - L_1)^2 + {r_3}^2}} \right), \tag{5}$$

where B_r is the remanence induction intensity of the permanent magnet ($B_r = \mu_0 M_0$), M_0 is the magnetization intensity of the permanent magnet, z_1 is the height of the permanent magnet axis, L_1 is the length of the permanent magnet, and r_3 is the radius of the permanent magnet. According to the Chinese sintered NdFeB permanent magnet material standard (GB/T 13560-2017), B_r is 1.23 T.

In order to calculate the interaction force between the energized coil and the permanent magnet, we regard the permanent magnet as a solenoid with turns n_m and current I_m ($M_0 = n_m I_m = 9.788 \times 10^5$ A/m) [34].

3) Force Analysis of the Probe in Different Positions: It can be seen from Fig. 1(b) that the probe is placed inside the upper frame and can only move up and down. When the beam drives the probe to move upward through the inclined structure under the action of electromagnetic force, the force of the beam and the probe is shown in Fig. 6. θ represents the angle between the slope and the horizontal plane, $\theta = 30°$. The following is the force analysis of the probe. When the beam moves horizontally to the right under the action of pushing force F_{a1}, the force acting on the probe through the inclined plane is F_{c2}. F_{c2} is perpendicular to the slope, and $F_{c2} = F_{a1}/sin\theta = 2F_{a1}$. By decomposing the force of F_{c2} in the horizontal and vertical directions, it can be obtained that the horizontal force of the probe squeezing the right support surface is F_{a2} ($F_{a1} = F_{a2} = F_{N2}$), and the total lifting force obtained by the probe is $F_{b2} = F_{a1}/tan\theta = \sqrt{3}F_{a1}$. According to the interaction of forces, the support force provided by the sleeve to the beam includes F_{N1} and F_{b1}, and $F_{N1} = G_1$, $F_{b1} = F_{b2} = \sqrt{3}F_{a1}$. Among them, G_1 is the total gravity of the beam, permanent magnet, probe and spring ($G_1 = 0.98$ mN). G_2 is the total gravity of the probe and spring ($G_2 = 0.2$ mN).

When the probe is at its lowest position, a forward current is applied to the coil, and the force F_{a1} acting on the beam can be expressed as:

$$F_{a1} = F_{coil1} - G_2 \tan\theta - f_1, \tag{6}$$

where F_{coil1} represents the repulsive force of the coil on the permanent magnet, and f_1 represents the friction force of the beam during the movement,

$$f_1 = \mu(F_{N1} + F_{b1}), \tag{7}$$

where μ is the dynamic friction coefficient. Through experimental measurement, it is concluded that the dynamic friction coefficient of the inclined plane made of resin is 0.1.

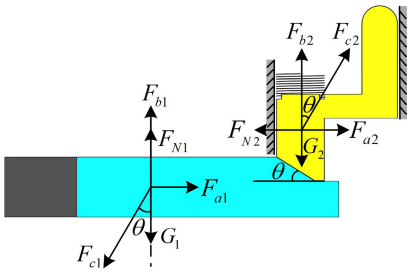

Fig. 6. Force analysis of the beam and the probe.

According to the structural parameters of Fig. 2, F_{coil1} can be calculated using the following equation [35]:

$$F_{\text{coil1}} = \frac{\mu_0 I_{\text{m}} n_m \pi r_3^2 N I}{2L(r_2 - r_1)} \times \left[\begin{array}{l} (z + \frac{L}{2} + \frac{L_1}{2}) \ln \frac{\sqrt{(z+\frac{L}{2}+\frac{L_1}{2})^2 + r_2^2} + r_2}{\sqrt{(z+\frac{L}{2}+\frac{L_1}{2})^2 + r_1^2} + r_1} \\ -(z + \frac{L}{2} - \frac{L_1}{2}) \ln \frac{\sqrt{(z+\frac{L}{2}-\frac{L_1}{2})^2 + r_2^2} + r_2}{\sqrt{(z+\frac{L}{2}-\frac{L_1}{2})^2 + r_1^2} + r_1} \\ -(z - \frac{L}{2} + \frac{L_1}{2}) \ln \frac{\sqrt{(z-\frac{L}{2}+\frac{L_1}{2})^2 + r_2^2} + r_2}{\sqrt{(z-\frac{L}{2}+\frac{L_1}{2})^2 + r_1^2} + r_1} \\ +(z - \frac{L}{2} - \frac{L_1}{2}) \ln \frac{\sqrt{(z-\frac{L}{2}-\frac{L_1}{2})^2 + r_2^2} + r_2}{\sqrt{(z-\frac{L}{2}-\frac{L_1}{2})^2 + r_1^2} + r_1} \end{array} \right]. \tag{8}$$

When the probe moves upward under the action of the inclined plane, the lifting force F_{up} of the Braille dot is:

$$F_{up} = F_{b2} - G_2 - kx - f_2, \tag{9}$$

where k is the stiffness coefficient of the spring (tested to be 150 N/m), x is the length of the spring being compressed, and f_2 is the friction force ($f_2 = \mu F_{N2}$) when the probe rises. When the probe is in the highest position, the compression of the spring is 0.1 mm, and the rebound force of the spring is 15 mN.

When the probe is reset, a reverse current is applied to the coil, and the force F_{a3} exerted on the beam can be expressed as:

$$F_{a3} = F_{coil2} + (G_2 + kx)\tan\theta - \mu G_1, \tag{10}$$

where F_{coil2} indicates the attraction of the permanent magnet during reset, and the calculation method of F_{coil2} is the same as that of F_{coil1}.

4) Finite Element Analysis: The electromagnetic force generated by the coil and the permanent magnet is converted into the lifting force of the probe through the slope. The lifting force refers to the force provided by the Braille dot during the ascent process, and the latching force refers to the force provided by the Braille dot when it is maintained at the highest position. The lifting force is usually less than the latching force. Considering that the Braille module designed in this study is a single "cell", the finger may not leave the contact surface in time during the process of Braille dot refresh. Therefore, in order to ensure that the state of the Braille dot can be correctly refreshed when the finger contacts the Braille dot, the probe needs to have a large lifting force to reach

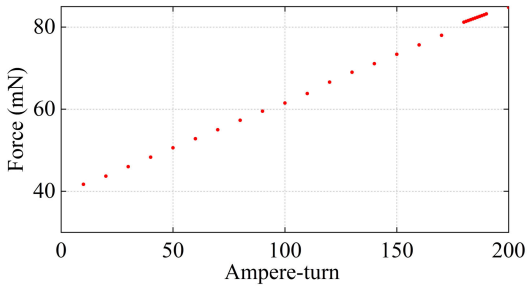

Fig. 7. The relationship between the maximum force of permanent magnet and *NI*.

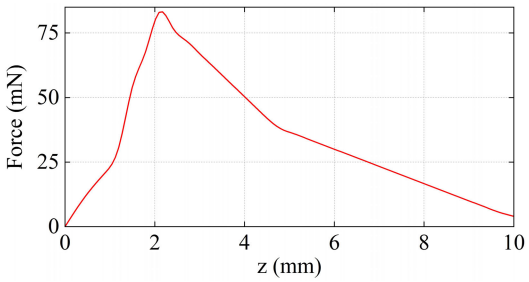

Fig. 8. Forces on permanent magnets at different positions.

the highest position smoothly. According to the requirement of literature [8] that the latching force should be greater than 100 mN, we set the target lifting force F_{up} to achieve the minimum latching force, that is, 100 mN.

In this paper, the finite element analysis is further employed to obtain the values of the parameters of the Braille dot actuator that meet the design requirements. The goal of finite element analysis is to ensure that the probe outputs the target lifting force while minimizing the volume and power consumption of the coil. Therefore, before the finite element analysis, we first specified the values of some parameters in Fig. 2 in order to quickly obtain the ideal actuator structure. Among them, r_1 is 1.8 mm, L is 3 mm, r_3 is 1 mm, L_1 is 3 mm. According to the lifting force F_{up} on the target of 100 mN, combined with equations (6), (7), and (9), F_{coil1} can be obtained as 83 mN.

Then, under the geometric model of Z-axis symmetry, we established a 2D structural model of the Braille dot actuator using ANSYS Maxwell software, and meshed and solved the model by setting appropriate boundary and excitation conditions. According to the results of Reference [35], the force-position relationship between the coil and the permanent magnet is an inverted parabola, indicating that the permanent magnet can obtain the maximum repulsion/attraction force at a certain position. In order to minimize the energy consumption of the coil, we hope that when the probe is just at its highest point, the force (F_{coil1}) of the permanent magnet reaches the maximum.

Since it is impossible to determine how large the magnetomotive force (NI) of the coil can cause the permanent magnet to be subjected to a maximum force of 83 mN, we apply an excitation to the coil from 0 to a maximum of 200 ampere-turn with a step of 10 ampere-turn. At the same time, under each excitation, we set the permanent magnet to move in a step size of 0.1 mm within the range of z from 0 to 10 mm. This can determine where the permanent magnet experiences the greatest repulsion/attraction force. The results of recording the maximum repulsion/attraction force of the permanent magnet under different excitations are shown in Fig. 7. It can be seen that when the magnetomotive force applied to the coil is 180-190 ampere-turn, the permanent magnet obtains a repulsion/attraction force of about 83 mN. In order to further determine the specific value of the magnetomotive force, we increase the excitation from 180 to 190 ampere-turn in a step of 1. Finally, it is determined that the repulsive/attractive force of the permanent magnet is 83 mN when the magnetomotive force is 189 ampere-turn and z is 2.1 mm. When the magnetomotive force is 189 ampere-turn, the force-z relationship during the movement of the permanent magnet is shown in Fig. 8.

In order to obtain the value of r_2, we put the determined F_{coil1}, z, NI into the equation (8), and calculate that r_2 is 3.61 mm. Due to the need to retain a certain installation space, we take r_2 as 3.75 mm. In addition, considering that the coil magnetic field generally has magnetic flux leakage, the actual magnetomotive force applied to the coil is determined to be $NI = (1 + 35\%) \times 189 = 255.15$ ampere-turn, and 255 ampere-turn are taken. Therefore, in the optimized coil space ($L = 3$ mm, $r_1 = 1.8$ mm, $r_2 = 3.75$ mm), we use enameled copper wire with a diameter of 0.15 mm to wrap 255 turns on the sleeve to make a coil, and input a maximum current of 1 A to the coil. The final structural parameters of the Braille dot actuator are shown in Table II. According to these specific structural parameters, we successfully fabricated the prototype of the Braille dot actuator and the Braille module, as shown in Fig. 9.

TABLE II
INTERNAL STRUCTURE PARAMETERS OF BRAILLE DOT ACTUATOR

Parameter	Identifier	Value
Inner coil radius (mm)	r_1	1.8
Outer coil radius (mm)	r_2	3.75
Coil length (mm)	L	3
Number of turns	N	255
Permanent magnet length (mm)	L_1	3
Permanent magnet radius (mm)	r_3	1
Maximum stroke of the permanent magnet (mm)	L_2	3

D. Performance Testing

The performance testing of the Braille dot actuator in this paper includes tests for the lifting force, latching force, and refresh frequency. The testing setup is shown in Fig. 10. A digital force gauge (ZTS-50N, Imada Inc., Japan) was fixed on an adjustable height test bench, with a force measurement range of -50 to 50 N and a resolution of 0.01 N. The probe of the force gauge is located directly above the Braille module.

During the testing for lifting force, we move the probe of digital force gauge to a position slightly smaller than 0.5 mm above the contact surface of the Braille module. Then drive a Braille dot, and the force values were recorded using the software provided with the force gauge. The test results of the

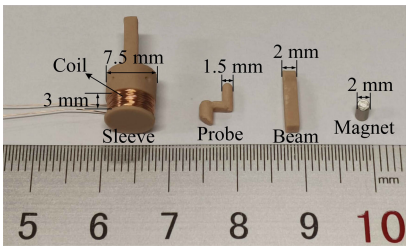

(a) Braille dot actuator

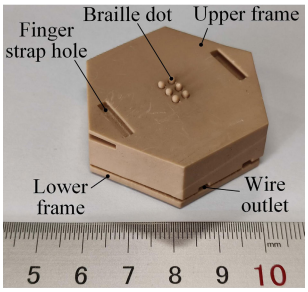

(b) Braille module

Fig. 9. Prototype dimensions and appearance.

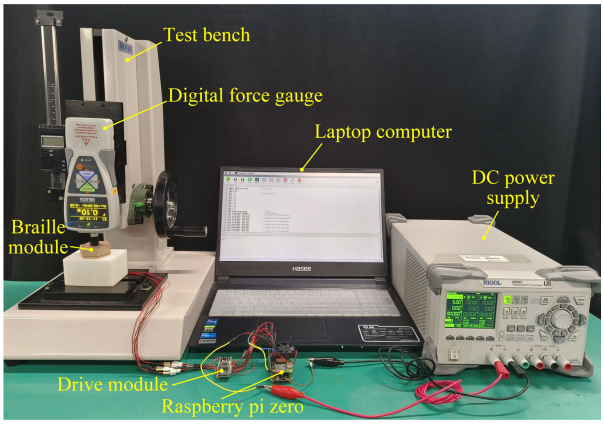

Fig. 10. Experimental platform for testing upper lifting force and latching force.

TABLE III
TEST RESULTS OF LIFTING FORCE ON 6 BRAILLE DOT ACTUATORS

Serial number	Lifting force (mN)
1	100
2	90
3	100
4	110
5	90
6	120

lifting force on the 6 Braille dot actuators are presented in Table III, indicating an average lifting force of 101.67 mN.

To prevent inadvertent depression of the raised Braille dots during reading, the Braille dot actuator must provide a protrusion latching force exceeding 100 mN [8]. When testing the latching force, the Braille dot was in the fully raised position, and pressure applied to the probe of the force gauge on the Braille dot was gradually increased. It was observed that even when the pressure reached 5 N, the Braille dot remained in the fully raised position. This indicates that the beam structure effectively supports the position of the Braille dot, ensuring complete latching.

TABLE IV
TEST RESULTS OF THE REFRESH FREQUENCY FOR 6 BRAILLE DOT ACTUATORS

Serial number	Cycle time (ms)	Refresh frequency (Hz)
1	58	17.2
2	57	17.5
3	59	16.9
4	61	16.4
5	59	16.9
6	57	17.5

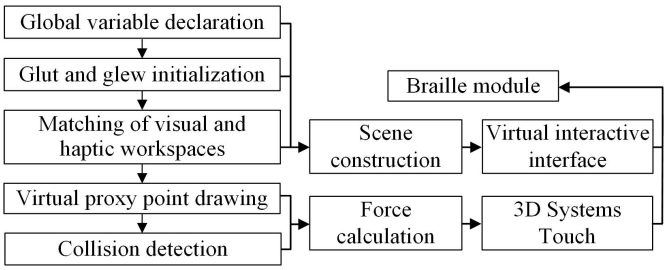

Fig. 11. Development architecture of virtual Braille interactive environment based on CHAI3D.

The refresh frequency of the Braille dot actuator directly determines the speed at which the Braille display device reproduces Braille. To meet the perceptual needs of BVI, the Braille display device should have a refresh frequency of at least 10 Hz [8]. When testing the refresh frequency, the Force Recorder Professional software, compatible with the ZTS-50N force gauge, was utilized to record the time from the moment of bounce to reset of braille dot within a cycle (with a sampling frequency of 1 kHz). Table IV shows the refresh frequencies of the 6 Braille dot actuators recorded in the test. It can be seen that the average refresh frequency of 17.1 Hz, which aligns with the design requirements.

III. DESIGN AND IMPLEMENTATION OF THE BRAILLE TOUCH-READING SYSTEM

A. Establishing a Virtual Braille Interaction Environment Based on CHAI3D

Drawing upon the customary reading motion of BVI, which involves touching Braille lines from left to right, this paper introduces a virtual Braille interaction environment within the CHAI3D framework. This environment simulates the distribution of Braille cells typically found on Braille book pages. Additionally, it utilizes the 3D Systems Touch device to enable BVI to read the virtual Braille content line by line. The CHAI3D stands out as one of the most widely used open-source frameworks for haptic interaction, supporting various commercial and customized force feedback devices. The Touch device features 3 degree-of-freedom (DoF) for force feedback and a 6-DoF position sensor, allowing precise measurement of the joystick's position and orientation in 3D space.

The development architecture of the virtual Braille interaction environment based on CHAI3D is illustrated in Fig. 11.

Initially, global variable declarations are made for the objects, processing routines, and parameters used in the program. Subsequently, initialization is carried out for Glut (OpenGL Utility Toolkit) and Glew (OpenGL Extension Wrangler), which includes window creation, initialization of window position and size, setting Glut callback functions, and related tasks. Additionally, the presence and initialization of Glew are also checked.

Visual and haptic workspace matching refers to the alignment of visual objects and haptic objects within the same coordinate system, ensuring that their perceptual ranges and accuracy correspond to each other. The process of rendering virtual proxy point includes the following steps: creating a haptic device handler, connecting the virtual proxy point to the Touch device. Subsequently, the virtual proxy point is inserted into the world and anchored at specific locations. Collision detection involves real-time tracking of the virtual proxy point's position and collision detection based on this positional information. If a collision event is detected, the system determines the collision point's location and applies external forces to the surrounding particles.

Scene construction involves the following steps. First, create the world and set the background color. Next, create a camera, insert it into the world, and fix its position. Then, create a light source, insert it into the world, and fix both its position and direction. In the interface, create nine attractive lines, configure their colors, magnetic attraction effects, and material properties. Afterward, create audio and load audio files, setting volume, speed, and playback mode. Finally, create a grid, load images, set their sizes, and fix their positions.

Force feedback computation involves the following steps. First, analyze the interactions between objects. Next, determine the way and intensity of force based on attributes such as the object's motion, shape, and material. Then, calculate information about the direction, magnitude, and point of action of the force feedback signal.

Following the aforementioned steps, we constructed a virtual Braille interaction interface, where each letter or symbol corresponds to a Braille cell. This interface mimics the layout and structure of actual Braille book pages, including text positioning and arrangement, laying the foundation for BVI to perform line-by-line touch-reading of virtual Braille.

B. Guided Reading Approach for Virtual Braille

Due to the inability to obtain visual information, BVIs face challenges in interacting with virtual Braille using the Touch device. To enable BVI to actively engage in line-by-line touch-reading of virtual Braille, this paper introduced the attraction constraint method from reference [28] into the CHAI3D virtual environment. Additionally, it designed a haptic rendering algorithm based on force-guidance mechanism. When a BVI picks up the joystick of the Touch device, the joystick applies active forces to guide the BVI's finger to the starting point of reading, which is the far-left of the first line of the Braille page. On each line of virtual braille, we have a line with attractive force, and the virtual proxy of the Touch device is constrained to this line when it comes into contact with the line. It prevents the proxy point from deviating and moving to other lines of Braille.

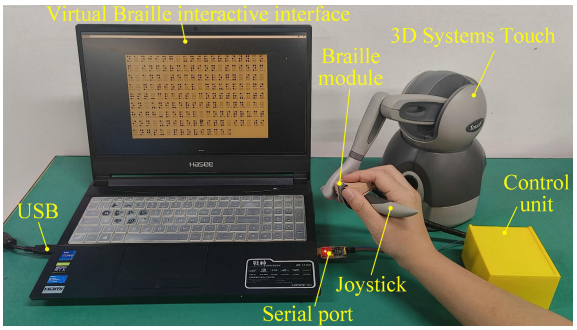

Fig. 12. Overall composition of the Braille touch-reading system.

When the proxy point reaches the far-right of a Braille line, it indicates that the line has been read, and the proxy point needs to transition to the next line or the far-left of the first line of the next page. To maintain the continuity of reading virtual Braille, the joystick actively guides the user's finger to initiate a new line under the influence of the force-guidance mechanism, allowing them to continue reading from the far-left of the next Braille line.

In the initialization phase, the desired position is set to the leftmost of the first line. When a BVI picks up the joystick, the haptic rendering algorithm calculates the traction force in real time and applies force to the finger through the joystick. The system adopts PID control algorithm to control the traction force exerted by the joystick. The direction of traction is the three-dimensional deviation direction of the desired position and the real-time position. During the traction process, the haptic rendering algorithm determines whether the distance between the desired position and the current position is less than the set value in real time. If it is less than the set value, the algorithm will interrupt the traction process, which means that the proxy point has reached the leftmost side of the first row. The algorithm resets the desired position to the leftmost of the second row. When the user moves the joystick from left to right to read the Braille, the algorithm will determine whether the proxy point reaches the rightmost side of the first row. If it reaches the rightmost side, the algorithm opens the traction program to move the finger to the leftmost side of the second row, so that BVI can continue reading.

C. The Working Principle of the Braille Touch-Reading System

Fig. 12 illustrates the overall composition of the Braille touch-reading system. Among them, the control unit integrates the Raspberry pi zero, driver module, power module, and a small fan. Fig. 13 shows the working principle of the system, with dashed lines representing power supply connections. This system communicates with the Raspberry pi zero via a serial interface and connects to the Touch device through a USB interface. The 6 output pins of the DRV8833 driver module are correspondingly connected to the positive and negative terminals of the 6 Braille actuators.

When BVI users use the system to perceive virtual Braille, the virtual proxy point moves to the corresponding Braille

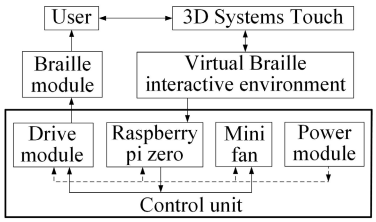

Fig. 13. Working Principles of the Braille touch-reading system.

cells. Subsequently, the system converts the respective virtual character into Braille encoding and sends it to the Raspberry pi zero via a serial connection. The Raspberry pi zero send instructions to the driver module, thereby outputting the appropriate current to drive the Braille dot actuators for the corresponding movement. When line change traction is required, the system sends commands to the Touch device via a USB interface to guide finger movement using the joystick.

IV. User Experiments of the Braille Touch-Reading System

To evaluate the effectiveness of the proposed Braille touch-reading system for BVI, we conducted four types of user experiments. We invited 10 blind subjects with at least 5 years of Braille learning experience to take part in the experiments, including 4 females, ranging in age from 18 to 28 years. These subjects usually use paper Braille books for reading. None of the subjects reported any deficiencies in their tactile perception abilities, and they were unaware of the purpose of the study. The experimental procedures received approval from our university's ethics committee.

Before the experiments commenced, we provided the subjects with a detailed introduction to the components of the Braille touch-reading system and the experimental procedure. Additionally, each subject underwent a training period. During this training, subjects learned how to navigate the virtual environment using the Touch device, how to tactilely read Braille information on the Braille module, and how to engage in digital Braille reading using the Braille touch-reading system. Any questions raised by the subjects during the training were clarified by the experimenter.

To assess whether subjects had learned how to use the proposed system, we provided them with different Braille content than what was used in the formal experiment. We recorded real-time 3D motion trajectory data as subjects manipulated the proxy point to perceive virtual Braille. We randomly selected a subject's 3D motion trajectory data during initial and proficient use of the system, as shown in Fig. 14. From the figure, it is evident that during the subject's initial use of the system, the motion trajectory was relatively chaotic, and there were improper operations such as jitter during line feed and proxy point separating from Braille line. After becoming proficient in using the system, the trajectory graph exhibited overall smoothness. This indicated that the subject was adept at operating the Touch device, correctly engaging in line-by-line tactile reading, and transitioning between lines. During the training period, each subject needed to demonstrate smooth

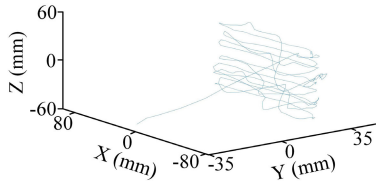

(a) Motion trajectory during initial use

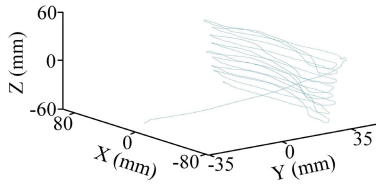

(b) Motion trajectory during proficiency use

Fig. 14. The 3D motion trajectory of the subject using the system.

motion trajectories to ensure that the performance evaluation of the Braille touch-reading system would not be influenced by proficiency level. All subjects confirmed their familiarity with the system's operation and the process of perceiving virtual Braille. They expressed confidence in their ability to understand Braille information, marking the end of the training process.

The experiment was conducted in four parts. In the Experiment 1, subjects read through paper Braille books. In the Experiment 2, subjects read Braille solely through the Braille module. In the Experiment 3, subjects used the proposed Braille touch-reading system, employing the Touch device to perceive Braille in the CHAI3D virtual environment. Experiment 4 added audio feedback to the Braille touch-reading system, enabling subjects to engage in multi-modal reading of virtual Braille.

A. Experimental Method and Procedure

In the experimental preparation phase, a subject sat at a table, donned the device, blindfold, and headphones playing white noise. We prepared a specific meaning sentence composed of 154 letters for each of the four experiments to assess how well subjects understood these sentences using the proposed Braille touch-reading system. A letter is displayed in a Braille cell. The content of the four sentences differed but posed an equivalent level of comprehension difficulty. The order in which subjects conducted the experiments was determined randomly by drawing lots. Each subject completed all four experiments. After completing each experiment, subject was required to describe to the experimenter what Braille content he/she had read. Experimenter then assessed reading accuracy based on the subject's descriptions. There was no time constraint on subject during the experiments, but the duration was recorded.

1) Experiment 1: In this experiment, as shown in Fig. 15(a), a Braille book was placed on the desktop. A subject used their fingertips to touch and read from left to right, and read line by line from top to bottom according to the layout order of the page. During the reading process, relative motion occurred between fingertip and Braille dots, and the subject

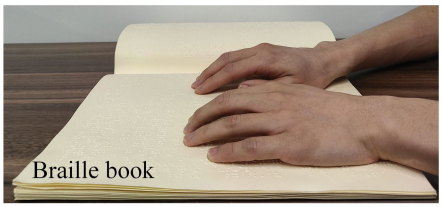

(a) A subject read a Braille book

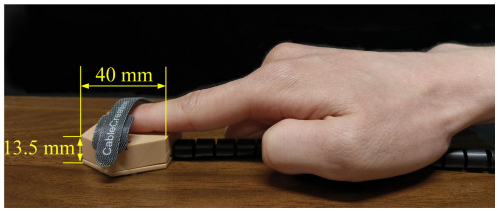

(b) A subject read Braille through the Braille module

Fig. 15. Experimental scenarios for Experiment 1 and Experiment 2.

obtained the Braille information by perceiving the distribution of the bumps. Subjects can move left and right freely on the Braille line until they have read the content composed of 154 letters. The experimenter rated the accuracy of the subject's description of the reading content and recorded the time spent.

2) Experiment 2: In this experiment, the Braille module was fixed to the tabletop, and a subject reads Braille in the manner shown in Fig. 15(b). The experimenter presented one Braille character at a time on the Braille module for subject to read. The subject can freely control the speed and pressure of the finger sliding across the Braille dots, and does not need to speak the perceived Braille information. Once they confirmed recognizing the Braille, subject informed the experimenter to proceed with the next Braille character. After all 154 Braille characters were presented to the subject in sequence, the experiment concluded. The experimenter assessed accuracy based on the subject's descriptions and recorded the time taken.

3) Experiment 3: In this experiment, the Braille module was securely fastened to the joystick using straps, as depicted in Fig. 12. The subject's thumb and middle finger could press against both sides of the Braille module to hold it in place. Simultaneously, subject used his/her index finger to read above the Braille module. This configuration did not impede the movement of the joystick or the subject's tactile perception of the Braille.

In this experiment, a subject utilized the joystick to navigate within the virtual Braille interaction interface. When the proxy point was positioned above the virtual Braille, the system would display the corresponding virtual Braille through the Braille module. The subject had the freedom to manipulate the proxy point, moving it left and right along a line of Braille, and when it reached the far-right end of a line, it was guided to the next line to continue reading, until all the content was read. Experimenter assessed accuracy based on subject's descriptions and recorded the time taken for reading.

4) Experiment 4: This experiment, building upon Experiment 3, introduced audio feedback to enable subject to engage

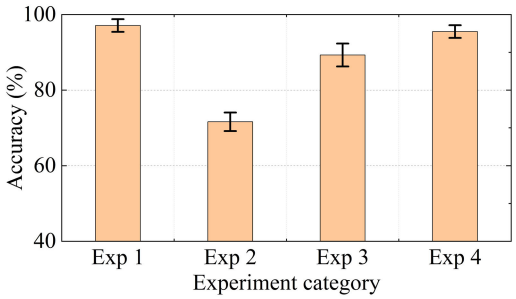

(a) Reading accuracy results

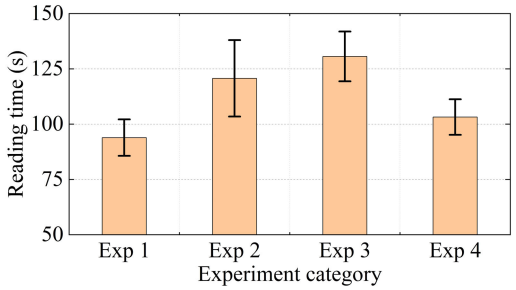

(b) Reading time results

Fig. 16. Statistics of results under different experimental conditions.

in multi-modal reading of virtual Braille. In the experiment, subject used the joystick to interact with virtual Braille. When the proxy point was positioned above the virtual Braille, the system not only displayed the virtual Braille on the Braille module but also played the corresponding letter pronunciation through the audio device. The remaining aspects of the experiment were consistent with Experiment 3.

B. Experimental Results

According to the above experimental procedures, the reading accuracy and time consumption of the subjects under different experimental conditions were counted respectively, as shown in Fig. 16(a) and Fig. 16(b). It can be seen that the average accuracy of the subjects in Experiment 1 reached the highest 97.1 % of the four experiments, and the average reading time was only 93.9 s. In Experiment 2, the average accuracy of reading through the Braille module was only 71.6 %, and the average reading time was 120.7 s. In contrast, the average accuracy of the subjects in Experiment 3 increased to 89.3 %, and the average reading time reached the longest 130.6 s in the four experiments. In Experiment 4, the average reading accuracy reached 95.5 % and the average reading time was 103.2 s through multi-modal feedback.

In order to further investigate the impact of differences in experimental conditions on subjects' reading of Braille, we first conducted normality and homogeneity tests on the data distribution of accuracy and time. After confirming that the data conforms to normality and homogeneity, we performed one-way analysis of variance (ANOVA) and post-hoc Tukey HSD multiple comparison tests (α=0.05) with respect to experimental conditions for accuracy and time, respectively. Fig. 17(a) and Fig. 17(b) respectively show the analysis results of the accuracy and time of perceiving Braille. In terms

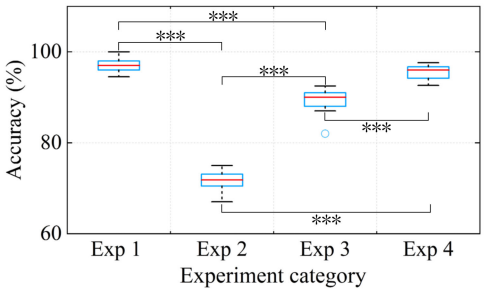

(a) Reading accuracy analysis

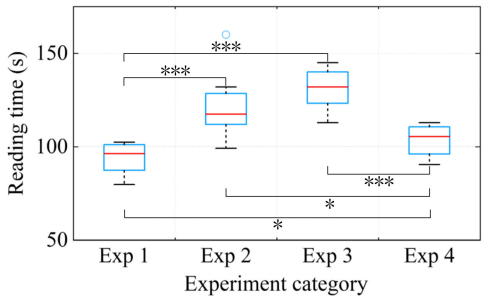

(b) Reading time analysis

Fig. 17. Analysis of results under different experimental conditions, where the markers (***), (*) indicate a significance of p≤0.001, p≤0.05, respectively.

of reading accuracy, different experimental conditions had a highly significant effect on the subjects reading of Braille ($F(3,36)=259.746$, $p<0.001$). Specifically, there was no statistically significant difference between Experiment 1 and Experiment 4 ($p=0.058$), and there were highly significant differences between the other experiments ($p<0.001$). In terms of reading time, different experimental conditions had a highly significant effect on the subjects reading of Braille ($F(3,36)=19.722$, $p<0.001$). Specifically, there was no statistically significant difference between Experiment 2 and Experiment 3 ($p=0.145$). There were certain differences between Experiment 1 and Experiment 4 ($p=0.02$), as well as between Experiment 2 and Experiment 4 ($p=0.013$). There were highly significant differences between the other experiments ($p<0.001$).

C. Subjective Evaluation Form

After the experiment, all 10 subjects were required to respond to the subjective evaluation form, with scoring criteria ranging from 1 (completely disagree) to 5 (completely agree). The questions and their average scores are presented in Table V. It can be observed that BVI subjects showed a strong interest in the proposed Braille touch-reading system and generally believed that the system has potential applications in their daily reading.

D. Discussion

This section investigates the effectiveness of the proposed Braille touch-reading system in facilitating digital reading for BVI through four experiments. The results of the post-hoc Tukey HSD multiple comparison test also showed a highly significant difference in reading accuracy between Experiment 2 and Experiment 3, but there was no statistically significant

TABLE V
SUBJECTIVE EVALUATION FORM

Questions	Average score
How familiar are you with Braille?	4.9
How often do you use Braille in your daily life?	4.6
How is the readability of the system?	4.5
How comfortable is the system?	4.4
How is the refresh frequency of the Braille module?	4.5
How is the latching force of the Braille module?	4.7
What do you think about the usability of this system?	4.6
Do you enjoy using this system?	4.8

difference in reading time. This could be attributed to the influence of the Braille exploration method. In Experiment 2, subjects could only read all Braille in sentence order, while in Experiment 3, they could repeatedly read one line of Braille. Due to the inability to review Braille that had already been read, some subjects reported being unable to accurately remember the content at the beginning of the sentence after completing Experiment 2. In Experiment 3, subjects could reread Braille by line in the virtual environment, reducing content forgetfulness during reading, thus enhancing reading accuracy. However, at the same time, reading time also increased.

Experiment 3 and Experiment 4 showed highly significant differences in both accuracy and time of reading. Compared with Experiment 3, the subjects significantly reduced their behavior of repeatedly reading a line of Braille in Experiment 4. The results showed that by synchronizing haptic and audio presentation of virtual Braille, subjects were able to understand the reading content faster and more deeply.

Experiment 1 and Experiment 4 showed no statistically significant difference in accuracy, but there was a certain difference in reading time. This indicates that although our proposed Braille touch-reading system can help BVI achieve accuracy similar to reading Braille books, the reading process is still somewhat complex.

From the subjective evaluations in Table V, it can be observed that subjects gave high ratings for the latching force and refresh frequency of the Braille module. After a period of experimentation, subjects expressed high satisfaction with the proposed system and considered it to be highly usable. The results from the experiments and subjective evaluations consistently indicate that the proposed Braille touch-reading system is effective in assisting BVIs with digital reading.

V. CONCLUSION

This paper presents a refreshable Braille display device designed for BVI digital reading. In conjunction with the Touch device and the CHAI3D virtual environment, a Braille touch-reading system has been developed. To provide substantial latching force to raised Braille dots without power consumption, this study designs a full latching Braille dot actuator based on Chinese Braille Standard. This actuator achieves complete latching of Braille dots after they are raised, ensuring accurate tactile perception for BVI. The Braille module features advantages such as high latching force, compact size, low power consumption, and low cost. When used by BVIs, they can freely control the speed and pressure of their fingers sliding over the Braille dots, enabling active tactile reading and improving Braille dot recognition accuracy.

The Braille touch-reading system is built upon CHAI3D, creating a virtual interactive interface that closely resembles real Braille book pages. It utilizes the Touch device to enable active tactile perception of virtual Braille for BVI, offering a more immersive and authentic reading experience. Combining tactile and audio modalities for Braille presentation deepens the understanding of touch content, consequently enhancing Braille recognition efficiency and reading speed for BVI. Performance tests and user experiments both indicate that the Braille touch-reading system developed in this study effectively assists BVI in Braille digital reading. This research provides an innovative solution for digitized reading by BVI and opens up promising applications for facilitating communication with digital information for BVI.

The Braille touch-reading system proposed in this paper still has room for improvement. First, the size of the control unit still needs to be further optimized to make it more compact and lightweight. Secondly, we recognize that the system presented in this paper may not cater to all the interaction needs of every BVI. In future work, we will conduct deeper research into the interaction methods between BVI and virtual environments to design Braille touch-reading system that better align with their unique interaction characteristics.

REFERENCES

[1] M. J. Burton et al., "The lancet global health commission on global eye health: Vision beyond 2020," *Lancet Glob. Health*, vol. 9, no. 4, pp. e489–e551, Apr. 2021.

[2] O. Ozioko, P. Karipoth, M. Hersh, and R. Dahiya, "Wearable assistive tactile communication interface based on integrated touch sensors and actuators," *IEEE Trans. Neural Syst. Rehabil. Eng.*, vol. 28, no. 6, pp. 1344–1352, Jun. 2020.

[3] N. Sribunruangrit, C. K. Marque, C. Lenay, S. Hanneton, O. Gapenne, and C. Vanhoutte, "Speed-accuracy tradeoff during performance of a tracking task without visual feedback," *IEEE Trans. Neural Syst. Rehabil. Eng.*, vol. 12, no. 1, pp. 131–139, Mar. 2004.

[4] D. Chen, J. Liu, L. Tian, X. Hu, and A. Song, "Research on the method of displaying the contour features of image to the visually impaired on the touch screen," *IEEE Trans. Neural Syst. Rehabil. Eng.*, vol. 29, pp. 2260–2270, 2021.

[5] X. Hu, A. Song, Z. Wei, and H. Zeng, "StereoPilot: A wearable target location system for blind and visually impaired using spatial audio rendering," *IEEE Trans. Neural Syst. Rehabil. Eng.*, vol. 30, pp. 1621–1630, 2022.

[6] J. Rantala et al., "Methods for presenting Braille characters on a mobile device with a touchscreen and tactile feedback," *IEEE Trans. Haptics*, vol. 2, no. 1, pp. 28–39, Jan. 2009.

[7] A. Russomanno, S. O'Modhrain, R. B. Gillespie, and M. W. M. Rodger, "Refreshing refreshable Braille displays," *IEEE Trans. Haptics*, vol. 8, no. 3, pp. 287–297, Jul. 2015.

[8] W. Yang, J. Huang, R. Wang, W. Zhang, H. Liu, and J. Xiao, "A survey on tactile displays for visually impaired people," *IEEE Trans. Haptics*, vol. 14, no. 4, pp. 712–721, Oct. 2021.

[9] Z. Zhou, Y. Yang, and H. Liu, "A Braille reading system based on electrotactile display with flexible electrode array," *IEEE/CAA J. Autom. Sinica*, vol. 9, no. 4, pp. 735–737, Apr. 2022.

[10] A. M. Echenique, J. P. Graffigna, and V. Mut, "Electrocutaneous stimulation system for Braille reading," in *Proc. Annu. Int. Conf. IEEE Eng. Med. Biol.*, Aug. 2010, pp. 5827–5830.

[11] Z. Liu, Y. Luo, J. Cordero, N. Zhao, and Y. Shen, "Finger-eye: A wearable text reading assistive system for the blind and visually impaired," in *Proc. IEEE Int. Conf. Real-Time Comput. Robot. (RCAR)*, Jun. 2016, pp. 123–128.

[12] A. Russomanno, R. B. Gillespie, S. O'Modhrain, and J. Barber, "Modeling pneumatic actuators for a refreshable tactile display," in *Proc. EuroHaptics*, 2014, pp. 385–393.

[13] X. Wu, S.-H. Kim, H. Zhu, C.-H. Ji, and M. G. Allen, "A refreshable Braille cell based on pneumatic microbubble actuators," *J. Microelectromech. Syst.*, vol. 21, no. 4, pp. 908–916, Aug. 2012.

[14] J. Yoo, S. Yun, S.-C. Lim, J. Park, K.-S. Yun, and H.-K. Lee, "Position controlled pneumatic tactile display for tangential stimulation of a finger pad," *Sens. Actuators A, Phys.*, vol. 229, pp. 15–22, Jun. 2015.

[15] C. W. Soule and N. Lazarus, "Reconfigurable Braille display with phase change locking," *Smart Mater. Struct.*, vol. 25, no. 7, Jul. 2016, Art. no. 075040.

[16] R. Velazquez, E. E. Pissaloux, M. Hafez, and J. Szewczyk, "Tactile rendering with shape-memory-alloy pin-matrix," *IEEE Trans. Instrum. Meas.*, vol. 57, no. 5, pp. 1051–1057, May 2008.

[17] G. Frediani, J. Busfield, and F. Carpi, "Enabling portable multiple-line refreshable Braille displays with electroactive elastomers," *Med. Eng. Phys.*, vol. 60, pp. 86–93, Oct. 2018.

[18] X. Qu et al., "Refreshable Braille display system based on triboelectric nanogenerator and dielectric elastomer," *Adv. Funct. Mater.*, vol. 31, no. 5, Jan. 2021, Art. no. 2006612.

[19] P. Chakraborti, H. A. K. Toprakci, P. Yang, N. Di Spigna, P. Franzon, and T. Ghosh, "A compact dielectric elastomer tubular actuator for refreshable Braille displays," *Sens. Actuators A, Phys.*, vol. 179, pp. 151–157, Jun. 2012.

[20] (2020). *Metec Ingenieur AG, Braille-Line-Flat 20*. [Online]. Available: https://www.metec-ag.de/downloads/braille-line-flat20.pdf

[21] V. Paneva, S. Seinfeld, M. Kraiczi, and J. Müller, "HaptiRead: Reading Braille as mid-air haptic information," in *Proc. ACM Designing Interact. Syst. Conf.*, Jul. 2020, pp. 13–20.

[22] H. Chen et al., "A novel refreshable Braille display based on the layered electromagnetic driving mechanism of Braille dots," *IEEE Trans. Haptics*, vol. 16, no. 1, pp. 96–105, Jan. 2023.

[23] G. C. Bettelani, G. Averta, M. G. Catalano, B. Leporini, and M. Bianchi, "Design and validation of the readable device: A single-cell electromagnetic refreshable Braille display," *IEEE Trans. Haptics*, vol. 13, no. 1, pp. 239–245, Jan. 2020.

[24] M. M. H. Saikot and K. R. I. Sanim, "Refreshable Braille display with adjustable cell size for learners with different tactile sensitivity," *IEEE Trans. Haptics*, vol. 15, no. 3, pp. 582–591, Jul. 2022.

[25] D. Leonardis, C. Loconsole, and A. Frisoli, "A passive and scalable magnetic mechanism for Braille cursor, an innovative refreshable Braille display," *Meccanica*, vol. 55, no. 8, pp. 1639–1653, Aug. 2020.

[26] J. Kim, B.-K. Han, D. Pyo, S. Ryu, H. Kim, and D.-S. Kwon, "Braille display for portable device using flip-latch structured electromagnetic actuator," *IEEE Trans. Haptics*, vol. 13, no. 1, pp. 59–65, Jan. 2020.

[27] (2023). *3D Systems Inc Touch*. [Online]. Available: https://www.3dsystems.com/haptics-devices/touch

[28] S. Paneels and J. C. Roberts, "Review of designs for haptic data visualization," *IEEE Trans. Haptics*, vol. 3, no. 2, pp. 119–137, Apr. 2010.

[29] J. P. Fritz and K. E. Barner, "Design of a haptic data visualization system for people with visual impairments," *IEEE Trans. Rehabil. Eng.*, vol. 7, no. 3, pp. 372–384, Sep. 1999.

[30] D. T. V. Pawluk, R. J. Adams, and R. Kitada, "Designing haptic assistive technology for individuals who are blind or visually impaired," *IEEE Trans. Haptics*, vol. 8, no. 3, pp. 258–278, Jul. 2015.

[31] W. Yu, R. Ramloll, and S. Brewster, "Haptic graphs for blind computer users," in *Proc. Int. Workshop Haptic Hum.-Computer Interact.*, 2000, pp. 41–51.

[32] M. Basharat, M. Ding, H. Cai, Y. Li, and J. Fang, "Design and analysis of multilayer solenoid coil for Faraday modulator," in *Proc. MATEC Web Conf.*, vol. 114, 2017, pp. 1–9.

[33] J. M. Camacho and V. Sosa, "Alternative method to calculate the magnetic field of permanent magnets with azimuthal symmetry," *Revista Mexicana de física E*, vol. 59, no. 1, pp. 8–17, 2013.

[34] M. Kwon, J. Jung, T. Jang, and S. Sohn, "Magnetic forces between a magnet and a solenoid," *Phys. Teacher*, vol. 58, no. 5, pp. 330–334, May 2020.

[35] H. Ha, T. Jang, S. H. Sohn, and J. Kim, "Magnetic force between a multilayered solenoid and a magnet," *Phys. Teacher*, vol. 60, no. 8, pp. 663–666, Nov. 2022.